Crowding Promotes the Switch from Hairpin to Pseudoknot Conformation in Human Telomerase RNA

Natalia A. Denesyuk and D. Thirumalai*

Department of Chemistry and Biochemistry and Biophysics Program, Institute for Physical Science and Technology, University of Maryland, College Park, Maryland 20742, United States

S *Supporting Information*

ABSTRACT: Formation of a pseudoknot (PK) in the conserved RNA core domain in the ribonucleoprotein human telomerase is required for function. In vitro experiments show that the PK is in equilibrium with an extended hairpin (HP) structure. We use molecular simulations of a coarse-grained model, which reproduces most of the salient features of the experimental melting profiles of PK and HP, to show that crowding enhances the stability of PK relative to HP in the wild type and in a mutant associated with dyskeratosis congenita. In monodisperse suspensions, small crowding particles increase the stability of compact structures to a greater extent than larger crowders. If the sizes of crowders in a binary mixture are smaller than that of the unfolded RNA, the increase in melting temperature due to the two components is additive. In a ternary mixture of crowders that are larger than the unfolded RNA, which mimics the composition of ribosome, large enzyme complexes and proteins in *Escherichia coli*, the marginal increase in stability is entirely determined by the smallest component. We predict that crowding can partially restore telomerase activity in mutants with decreased PK stability.

Despite the recognition that macromolecular crowding could affect a variety of biological functions,[1] including folding and catalysis by both proteins and RNA, efforts to understand the influence of crowding on RNA have just begun.[2] In many situations RNA molecules, such as riboswitches,[3] undergo a transition between two distinct conformations that have a profound influence on their functions. An example of interest here is the conformational switch in the pseudoknot domain of telomerase RNA, which is conserved in ciliates, yeast and vertebrates and whose activity is closely linked to chromosome stability.[4] Although the assembly and function of telomerase requires that this domain adopt a pseudoknot (PK) conformation in vivo,[5] structural analysis using chemical foot printing failed to detect stable PK structure in human telomerase RNA (hTR).[6] Subsequently, NMR structures showed evidence for a molecular switch between PK and hairpin (HP) conformations,[7] which is linked to in vivo function of telomerase.[8] Mutations that either increase or decrease the stability of the PK result in a reduction in telomerase activity. Physical factors such as temperature or crowding in the cellular environment, may also influence the PK−HP equilibrium, thus regulating telomerase activity. In this theoretical study we investigate how molecular crowding influences the switch between PK and HP and assess the implications of our findings for telomerase activity in mutants linked to diseases.

The high density of macromolecules in the cell (volume fractions $\varphi \approx 0.2-0.4$) reduces the space available for conformational fluctuations, which should result in a shift in the thermodynamic equilibrium toward the more compact PK. To assess the extent to which PK is favored at $\varphi \neq 0$, we simulate the modified hTR pseudoknot domain, which has been examined experimentally in vitro at $\varphi = 0$ in the wild type (WT) and the mutant ΔU177 (deleted U177).[8b] Because the structures of WT and ΔU177 are similar, we expect that crowding effects will be quantitatively comparable in both cases. Here we present simulation results for ΔU177, whose PK and HP structures (Figure 1) are available from the Protein Data Bank, codes 2K96 and 1NA2.

We performed coarse-grained[10] Langevin dynamics simulations of PK and HP using a novel force field based on the three interaction site (TIS) model,[10a] in which each nucleotide is replaced by three beads: ribose, base and phosphate. Interactions maintaining the structures are bond length and angle constraints, single-strand base stacking and interstrand hydrogen bonding (see Supporting Information (SI)). The force field parameters are derived from experimental data (details in SI). We obtained stacking parameters for all possible nucleotide dimers from thermodynamic measurements on the formation of single and double helices in RNA at monovalent salt concentrations $c_M = 1$ M.[11] Our stacking parameters are quantitatively valid for sufficiently high c_M, such that the electrostatic forces between phosphates can be neglected. To model hydrogen bonding, we generated an optimal network of atomistic hydrogen bonds in the PDB structure of PK or HP using the WHAT IF server at http://swift.cmbi.ru.nl. The generated bonds are mapped onto multibody potentials that are applied to the coarse-grained beads. The present force field makes it possible to obtain stable helical geometries. Good agreement between the simulation and experimental results for folding thermodynamics at $\varphi = 0$ validates our model.

The simulated melting curve of PK at $\varphi = 0$ has a sharp peak at $t = 70$ °C (Figure 2a, black), in agreement with experimental UV melting data.[8b] The position of this peak is determined primarily by stem 2, whose melting profile also peaks at 70 °C (Figure 2a, blue). At $t > 80$ °C, stem 2 is entirely melted (the number of intact base pairs $N_{BP} = 0$), and the overall melting curve is dominated by stem 1. Despite being shorter than stem 2, stem 1 fully melts only at 100 °C due to a high G−C content (Figure 2a, red). The simulated thermodynamic data are in agreement with experiments.[8b] The tertiary structure of PK melts in the temperature range 60−80 °C (Figure 2a, orange), as does stem 2,
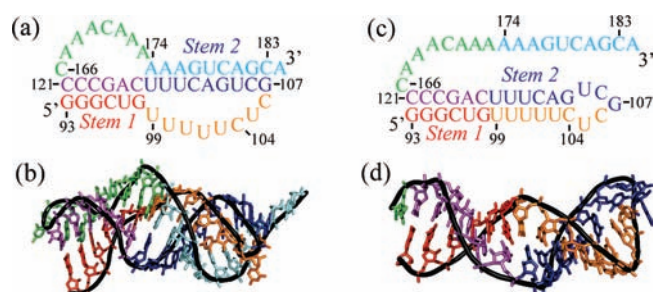
Figure 1. Secondary and tertiary structures of PK (a, b) and HP (c, d) for ΔU177. Nucleotides 122−165 and 177 are deleted in this construct. (a) PK secondary structure includes a six base pair stem 1 (red and magenta) and a nine base pair stem 2 (blue and cyan). (b) PK tertiary structure has a Hoogsteen base pair, U99●−■A173, and six stacked base triples: U100●−■A174−U115, U101●−■A175−U114, U102●−■A176−U113, A172○−△G98═C116, A171○−△U97═A117, and A169□−△G118═C96 (see ref 9 for symbols designating various base pair families). (c) HP has a double helix with six Watson−Crick base pairs in common with stem 1 in PK, two additional Watson−Crick base pairs, A111−U103 and G110═C104, and four noncanonical base pairs, U99-●-U115, U100-●-U114, U101-●-U113 and U102-●-C112. (d) NMR structure of HP includes residues G93 to C166 only. To quantify the effect of crowders on the stability of HP, we added an unstructured tail A167−A184 (c) to the NMR structure.
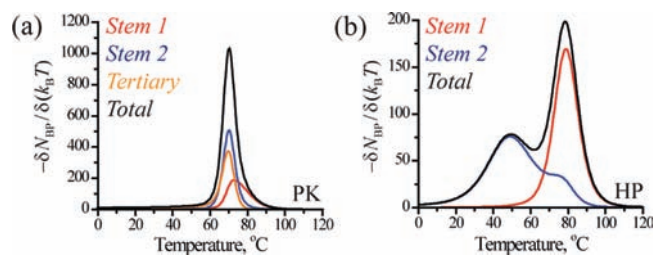

Figure 2. Negative derivative of the number of intact base pairs N_{BP} with respect to $k_B T$, as a function of temperature, for PK (a) and HP (b). k_B is the Boltzmann constant in kcal/(mol·K), T is the absolute temperature in K. Shown are the partial contributions of the structural elements defined in Figure 1, as well as the total contributions of all base pairs.

since the formation of stem 2 ensures the spatial proximity of the elements of the tertiary structure. In experiments, however, the tertiary structure melts over a broader temperature range (40−80 °C)[8b] than our simulation results indicate.

The melting curve of HP, obtained using the same set of simulation parameters as for PK, has two distinct peaks at 50 and 78 °C (Figure 2b, black), in agreement with the experimental peaks at 50 and 79 °C.[7] The peaks correspond to melting of U-rich stem 2 and of Watson−Crick stem 1 (Figure 1). Since isolated uridine dimers have not been observed to stack at $t > 0$ °C,[11a] stem 2 must be stabilized almost exclusively by hydrogen bonds, which explains the low melting temperature.

We define the stability $\Delta G(\varphi)$ of each structure as the free energy difference between ensembles sampled at 0 and 120 °C. For 0 °C $< t <$ 120 °C, $\Delta G(\varphi)$ is computed using an analogue of the weighted histogram method.[12] For PK at 37 °C we obtain $\Delta G_{PK}(0) = -21.5$ kcal/mol (Figure S5a, SI). The experimental value is −22.9 kcal/mol.[8b] The stability of PK with respect to HP, $\Delta G_{PK}(0) - \Delta G_{HP}(0)$, is −8.3 kcal/mol at 37 °C, confirming that PK is the predominant structure of the ΔU177 mutant. However, PK shows a more rapid decrease in stability with temperature, indicating a larger entropy loss associated with the folding of
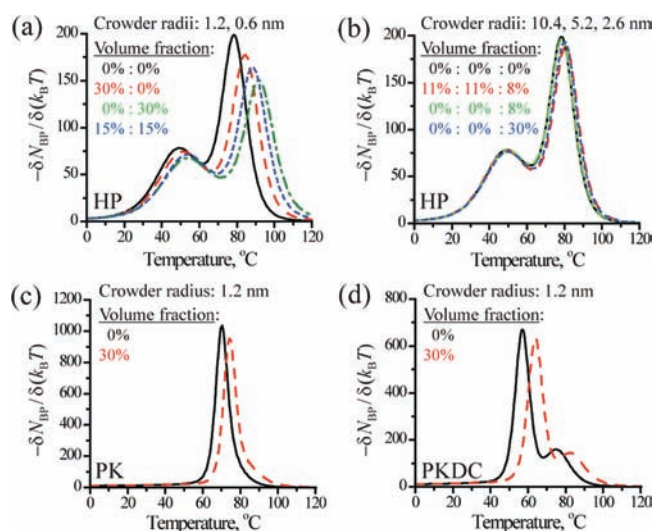

Figure 3. Melting profiles of HP (a, b), PK (c) and PKDC (d) in various mixtures of crowders. The red dashed curve in (b) corresponds to the *E. coli* mixture. Two melting peaks in (d) are due to stems 1 and 2.

the PK. Part of the entropy loss in PK results from the tight turn at C166 and binding of strand C166−A184 to the rest of the structure. Another entropic contribution is due to the stacking of bases in stem 2 in PK, which is longer than stem 2 in HP and includes stacks with strong temperature dependence (see SI). In contrast to PK, strand C166−A184 in HP does not form hydrogen bonds with the rest of the molecule and adopts more extended conformations, which should be inhibited at $\varphi \neq 0$ due to reduction in volume accessible to RNA. We therefore expect that in the presence of crowders the entropy loss associated with the binding of strand C166−A184 to the rest of the structure will decrease and the PK−HP equilibrium will shift toward PK. To test this notion, we carried out simulations of HP and PK in suspensions of spherical crowding particles with different radii.

The melting profiles of HP in different crowder mixtures (Figure 3a,b) show that the magnitude of the crowding effect is strongly dependent on the size of the crowding particle. The curves in Figure 3a, which correspond to crowder radii r_C that are smaller than the radius of gyration of strand G93−C121 in the unfolded state, $R_G^0 = 2$ nm, show significant changes at $\varphi = 0.3$. The melting temperature of stem 1 in HP increases from 78 to 84 °C for $r_C = 1.2$ nm and to 91 °C for $r_C = 0.6$ nm. The influence of crowders on the melting of stem 2 in HP is less pronounced because U-rich stem 2 is relatively weak and melts at a lower temperature than stem 1. If stem 1 is intact, melting of stem 2 will not result in substantial change in the RNA molecule's size. The main influence of crowding on folding/unfolding comes through suppression of extended conformations which are prevalent in the unfolded state. Consistent with the entropic stabilization mechanism,[1c] we find that the effect of crowders on the unfolding of stem 2 is not significant, since such unfolding does not result in formation of extended conformations with high probability.

We also considered a binary mixture containing a volume fraction $\varphi = 0.15$ of crowders with $r_C = 1.2$ nm and a similar volume fraction of crowders with $r_C = 0.6$ nm (the total volume fraction $\varphi_T = 0.3$). In the mixture, the melting temperature of stem 1 in HP increases from 78 to 88 °C, compared to 84 and 91 °C in monodisperse suspensions with $\varphi = 0.3$ and $r_C = 1.2$ or 0.6 nm, respectively (Figure 3a). If crowders are small relative to RNA, their mixing is homogeneous on the length scales relevant

for the folding/unfolding transition. In this case, the crowding effect of a mixture should be an average of the effects due to the monodisperse components. In accord with this expectation we find that the increase in the melting temperature ΔT is given by $\varphi_T \Delta T = \varphi_1 \Delta T_1 + \varphi_2 \Delta T_2$, where $\varphi_T = \varphi_1 + \varphi_2$ and $\Delta T_1, \Delta T_2$ are computed for monodisperse suspensions 1 and 2 with $\varphi = \varphi_T$.

In Figure 3b we show the melting profiles of HP in mixtures of crowders with radii $r_C > R_G^0$. The effects of large crowders on the melting of HP are minimal, even at $\varphi = 0.3$. If φ is fixed, the average distance between two spherical crowders will increase with the crowder size. If RNA molecule fits into available space in both folded and unfolded states, the folding/unfolding transition will not be affected significantly by the presence of crowders. Even for a crowder radius only slightly larger than R_G^0, $r_C = 2.6$ nm, the increase ΔT in the melting temperature of stem 1 in HP is not greater than 1.5 °C (Figure 3b). Further increase in r_C results in $\Delta T \approx 0$ at $\varphi = 0.3$. Hence, as predicted qualitatively using concepts in colloid science,[13] small crowders (or more precisely $r_C/R_G^0 < 1$) have the largest stabilizing effect.

Figure 3b also shows the melting profile of HP in a ternary mixture of crowders, which contains volume fractions $\varphi = 0.11$, 0.11, and 0.08 of particles with $r_C = 10.4$ nm, 5.2 and 2.6 nm, respectively. The sizes and concentrations of individual components in this mixture are chosen to model ribosome, large enzymatic complexes and relatively small individual proteins found in *E. coli*. Because the radii of all the components in the *E. coli* mixture are larger than R_G^0, we expect only small changes in the melting profile of HP (Figure 3b). For $\varphi_T = 0.3$, the melting temperature of stem 1 in HP increases only by 2 °C. Interestingly, the *E. coli* mixture has a similar effect on the melting of HP as a monodisperse suspension with $r_C = 2.6$ nm and $\varphi = \varphi_T$. By contrast, a monodisperse suspension with $r_C = 2.6$ nm and $\varphi = 0.08$, which equals this component's volume fraction in the mixture, has no effect on the melting of HP (Figure 3b). This implies that in polydisperse mixtures of crowders with very different radii the large crowding particles act like immobile obstacles separating the available space into compartments filled with smaller crowders. The effective volume fraction of small crowders within the compartments will roughly equal φ_T of all crowders in the mixture. Thus, the influence of such polydisperse mixtures will be comparable to the effect of the smallest component calculated at volume fraction φ_T. We note that the situation here is different from the binary mixture of small crowders considered above, where the particle sizes and masses are such that the mixture appears entirely homogeneous on the length and time scales relevant to the folding/unfolding transition. In that case, the magnitude of the crowding effect is determined not by the smallest component but by both components equally (Figure 3a).

The results in Figure 3b suggest that the effect of crowding in vivo is determined by the heterogeneity of the environment. Inhomogeneous distribution of biomaterials in cells has long been recognized and termed "microcompartmentation".[14] The effect of crowding on biomolecular processes may vary strongly in different regions of the cell, depending on local concentrations and sizes of the crowding macromolecules. Furthermore, large and heavy components, such as ribosomes, which are relatively immobile on the time scales relevant to many processes, may create dynamic inhomogeneities in cells (similar to phenomena in supercooled liquids[15]) that will have a different impact on the same cellular process at distinct times.

Even for monodisperse crowders studied in vitro, a single variable φ is not sufficient for a quantitative description of the crowding
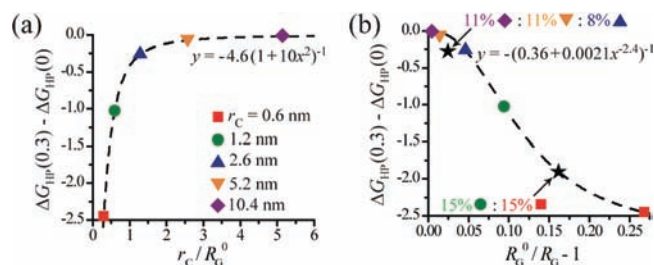

Figure 4. Change in stability (in kcal/mol) of HP at 37 °C due to crowders, shown in (a) vs the crowder radius, r_C, and in (b) vs $R_G^0/R_G - 1$. Colored symbols mark monodisperse crowder suspensions with $\varphi = 0.3$ and r_C indicated in left panel; ($\star$) corresponds to polydisperse mixtures with volume fractions indicated in the right panel. (- - -) fits to specified rational functions.

effect on the PK−HP equilibrium. Figure 4a shows the change in stability of HP at 37 °C induced by monodisperse crowders with $\varphi = 0.3$, for different crowder radii. The excess stability $\Delta G_{HP}(0.3) - \Delta G_{HP}(0)$ is small if $r_C/R_G^0 > 1$ and increases sharply for $r_C/R_G^0 < 1$, consistent with the discussion above.

To address the mechanism of crowder-induced stabilization, we show in Figure 4b $\Delta G_{HP}(0.3) - \Delta G_{HP}(0)$ as a function of the deviation of the radius of gyration of an unfolded hairpin (strand G93−C121) in the presence of crowders, R_G, from its value in the absence of crowders, R_G^0. The stability of HP increases with the ratio R_G^0/R_G, which in turn increases with decreasing the crowder radius r_C. Simulation data that couple r_C to the size and stability of PK are shown in Figure S6. All data confirm that the crowders reduce the conformational space accessible to the unfolded state by suppressing some of the most expanded conformations. The same arguments hold for polydisperse mixtures, where the magnitude of the stabilization effect due to crowders is also related to changes in R_G (Figure 4b). Decreasing ionic strength will enhance the crowding effect by increasing R_G of the unfolded RNA. However, this enhancement should not be significant in vivo, since the electrostatic forces between phosphates are largely screened at $c_M \approx 0.2$ M.

We explore the crowding-facilitated switch between PK and HP in a suspension of crowders with radius $r_C = 1.2$ nm and $\varphi = 0.3$. In the presence of crowders, the melting temperature of PK increases from 70 to 74 °C (Figure 3c), whereas the individual melting peak of stem 1 shifts to higher temperatures by as much as 9 °C (Figure S7). Unfolding of stem 1 is the last step in the melting of PK, which leads to a complete opening of the structure and results in a significant increase in R_G. The size of an unfolded molecule is directly coupled to the magnitude of the crowding effect, which explains a large impact of crowders on the unfolding of stem 1.

For $r_C = 1.2$ nm and $\varphi = 0.3$, the stabilities of PK and HP in the temperature range 0−120 °C are compared in Figure S5a. At 37 °C, $\Delta G_{PK}(0.3) - \Delta G_{PK}(0) = -2.4$ kcal/mol and $\Delta G_{HP}(0.3) - \Delta G_{HP}(0) = -1.0$ kcal/mol, indicating an equilibrium shift toward PK. The observed change in the PK−HP relative stability by -1.4 kcal/mol is associated with the binding of strand C166−A184 to the remainder of the structure in PK, whose release is inhibited in a crowded environment.

To confirm that the crowding effect depends on RNA size rather than sequence, we simulated the ΔU177 mutant with two additional mutations, GC107/8 → AG, linked to dyskeratosis congenita (DKC). The DKC mutations reduce the stability of stem 2 in the pseudoknot (PKDC, Figure 3d), yielding $\Delta G_{PKDC}(0) = -16.4$ kcal/mol at 37 °C (the experimental value is -16.3 kcal/mol[8b]).
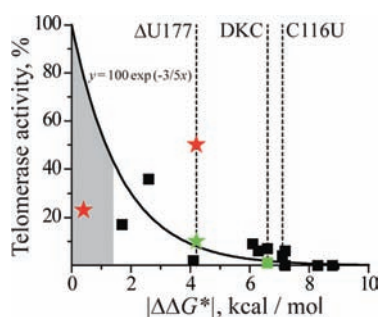
Figure 5. Activity of mutant telomerase normalized to wild-type activity (100%), plotted vs the absolute value of the stability difference between mutant and wild-type PKs. The in vitro data for $\Delta\Delta G^* > 0$ ($\blacksquare$) and $\Delta\Delta G^* < 0$ (red $\star$) are from Table 2 in ref 8b. Mutants $\Delta U177$, DKC, and C116U are explicitly marked. In vivo data for $\Delta U177$ and DKC from ref 8a are indicated by green symbols; the activity of these mutants in vivo is lower than in vitro. In vivo, DKC mutation reduces telomerase activity >100-fold,[8a] shown as 1% in the figure. Solid curve shows the specified exponential function. Gray area marks the range of potential mutants whose activity may be up-regulated by crowding.

Thermodynamic properties of the hairpin (HPDC) change insignificantly in the DKC relative to the wild type (Figure S8). The resulting stability of PKDC relative to HPDC is only -3.0 kcal/mol at 37 °C (or smaller without the $\Delta U177$ mutation). For the DKC mutant in a suspension of crowders with $r_C = 1.2$ nm and $\varphi = 0.3$, the excess stabilities of PKDC and HPDC are -2.8 and -1.2 kcal/mol, respectively (Figure S5b). These values are marginally larger than those obtained for PK and HP. Thus, our estimates of the stability changes due to crowders apply to all mutants for which the structures of the PK and HP structures are preserved.

Our finding that PK formation is promoted by crowding can be used to assess the extent to which macromolecules can regulate telomerase activity. Experimental data[8] (Figure 5) show that enzyme activity decreases when plotted as a function of $|\Delta\Delta G^*| = |\Delta G^*_{PK}(0) - \Delta G_{PK}(0)|$, where $\Delta G^*_{PK}(0)$ and $\Delta G_{PK}(0)$ are the respective stabilities of mutant and wild-type pseudoknots at $\varphi = 0$. Majority of mutations destabilize the PK, $\Delta\Delta G^* > 0$ ($\blacksquare$ in Figure 5) and only two mutants have $\Delta\Delta G^* < 0$ (red $\star$ in Figure 5). For the destabilizing mutants, reduction in activity α is approximately described as $\alpha = \exp(-3/5\Delta\Delta G^*)$ (thick curve in Figure 5). We obtain this formula by fitting the experimental data to exponential decay, assuming $\alpha = 1$ at $\Delta\Delta G^* = 0$ (wild type). The destabilizing DKC and the stabilizing $\Delta U177$ mutations have been studied in vivo[8a] (green symbols in Figure 5), as well as in vitro.[8b] In both cases, mutant telomerase in vivo was at least 5 times less active than the in vitro counterpart, suggesting that additional factors may influence the activity of telomerase in vivo. The double mutant GC182/3 $\rightarrow$ CU, compensatory to DKC, was shown to partially restore telomerase activity in vivo.[8a] We attribute the decrease in α to the reduced stability of the pseudoknot in the quadruple mutant, $\Delta\Delta G^* = 1.2$ kcal/mol, as predicted from RNA stacking parameters in ref 11b. On the basis of the formula $\alpha = \exp(-3/5\Delta\Delta G^*)$, we estimate activity of the quadruple mutant to be less than 50% of the maximum activity.

Although crowding enhances the stability of the PK, the effect is smaller (for typical crowder sizes $r_C > 1$ nm) than the stability changes caused by mutations. In Figure 5 the gray area marks the range of potential mutants with $\Delta\Delta G^* > 0$, whose activity could be restored by crowding alone. All experimentally studied mutants, for which $\Delta\Delta G^* > 0$, fall outside the marked region, including the two naturally occurring disease-related mutants DKC and C116.

Nevertheless, due to the exponential dependence of α on $\Delta\Delta G^*$, the effect of crowding on telomerase function can be substantial. We estimate that the activity of telomerase can be up- or down-regulated by more than 2-fold, by modulating the density of crowders in the cellular environment. Furthermore, due to the expected dynamical heterogeneities in cells, there will be variations in α in different cell regions. In light of our findings it is of interest to study how riboswitches, which undergo a switch in conformation in response to metabolite binding, adapt to function in their local cellular environment.

■ ASSOCIATED CONTENT

ⓢ Supporting Information. Experimental details. This material is available free of charge via the Internet at http://pubs.acs.org.

■ AUTHOR INFORMATION

Corresponding Author
thirum@umd.edu

■ ACKNOWLEDGMENT

■ REFERENCES

(1) (a) Zhou, H.-X.; Rivas, G.; Minton, A. P. *Ann. Rev. Biophys.* **2008**, *37*, 375. (b) McGuffee, S. R.; Elcock, A. H. *PLoS Comput. Biol.* **2010**, *6*, e1000694. (c) Cheung, M. S.; Klimov, D.; Thirumalai, D. *Proc. Natl. Acad. Sci. U.S.A* **2005**, *102*, 4753. (d) Dhar, A.; Samiotakis, A.; Ebbinghaus, S.; Nienhaus, L.; Homouz, D.; Gruebele, M.; Cheung, M. S. *Proc. Natl. Acad. Sci. U.S.A* **2010**, *107*, 17586.

(2) (a) Pincus, D. L.; Hyeon, C.; Thirumalai, D. *J. Am. Chem. Soc.* **2008**, *130*, 7364. (b) Kilburn, D.; Roh, J. H.; Guo, L.; Briber, R. M.; Woodson, S. A. *J. Am. Chem. Soc.* **2010**, *132*, 8690.

(3) Montange, R. K.; Batey, R. T. *Ann. Rev. Biophys.* **2008**, *37*, 117.

(4) (a) Chen, J. L.; Greider, C. W. *Proc. Natl. Acad. Sci. U.S.A* **2004**, *101*, 14683. (b) Blasco, M. A. *Curr. Opin. Genet. Dev. U.S.A* **2003**, *13*, 70.

(5) Gilley, D.; Blackburn, E. H. *Proc. Natl. Acad. Sci. U.S.A* **1999**, *96*, 6621.

(6) Antal, M.; Boros, E.; Solymosy, F.; Kiss, T. *Nucleic Acids Res.* **2002**, *30*, 912.

(7) Theimer, C. A.; Finger, L. D.; Trantirek, L.; Feigon, J. *Proc. Natl. Acad. Sci. U.S.A* **2003**, *100*, 449.

(8) (a) Comolli, L. R.; Smirnov, I.; Xu, L.; Blackburn, E. H.; James, T. L. *Proc. Natl. Acad. Sci. U.S.A* **2002**, *99*, 16998. (b) Theimer, C. A.; Blois, C. A.; Feigon, J. *Mol. Cell* **2005**, *17*, 671.

(9) Leontis, N. B.; Stombaugh, J.; Westhof, E. *Nucleic Acids Res.* **2002**, *30*, 3497.

(10) (a) Hyeon, C.; Thirumalai, D. *Proc. Natl. Acad. Sci. U.S.A* **2005**, *102*, 6789. (b) Whitford, P. C.; Schug, A.; Saunders, J.; Hennelly, S. P.; Onuchic, J. N.; Sanbonmatsu, K. Y. *Biophys. J.* **2009**, *96*, L7. (c) Feng, J.; Walter, N. G.; Brooks, C. L., III. *J. Am. Chem. Soc.* **2011**, *133*, 4196. (d) Lin, J. C.; Thirumalai, D. *J. Am. Chem. Soc.* **2008**, *130*, 14080. (e) Cao, S.; Chen, S. J. *J. Mol. Biol.* **2007**, *367*, 909. (f) Cao, S.; Giedroc, D. P.; Chen, S. J. *RNA* **2010**, *16*, 538.

(11) (a) Bloomfield, V. A.; Crothers, D. M.; Tinoco, I., Jr. *Nucleic Acids: Structures, Properties, and Functions*, 1st ed.; University Science Books: Mill Valley, CA, 2000. (b) Xia, T.; SantaLucia, J., Jr.; Burkard, M. E.; Kierzek, R.; Schroeder, S. J.; Jiao, X.; Cox, C.; Turner, D. H. *Biochemistry* **1998**, *37*, 14719.

(12) Denesyuk, N. A.; Weeks, J. D. *Phys. Rev. Lett.* **2009**, *102*, 108101.

(13) (a) Asakura, S.; Oosawa, F. *J. Chem. Phys.* **1954**, *22*, 1255. (b) Shaw, M. R.; Thirumalai, D. *Phys. Rev. A* **1991**, *44*, 4797.

(14) Walter, H.; Brooks, D. E. *FEBS Lett.* **1995**, *361*, 135.

(15) Thirumalai, D.; Mountain, R. D.; Kirkpatrick, T. R. *Phys. Rev. A* **1989**, *39*, 3563. Kirkpatrick, T. R.; Thirumalai, D. *J. Phys. A* **1989**, *22*, L149.